Soft Matter

No unjamming transition in a Voronoi model of biological tissue

Journal:	*Soft Matter*
Manuscript ID	SM-ART-10-2017-002127.R2
Article Type:	Paper
Date Submitted by the Author:	02-Apr-2018
Complete List of Authors:	Sussman, Daniel; Syracuse University Merkel, Matthias; Syracuse University, Department of Physics

Journal Name

ARTICLE TYPE

Cite this: DOI: 10.1039/xxxxxxxxxx

No unjamming transition in a Voronoi model of biological tissue

Daniel M. Sussman*[a‡] and Matthias Merkel[a‡]

Received Date
Accepted Date

DOI: 10.1039/xxxxxxxxxx

www.rsc.org/journalname

Vertex models are a popular approach to simulating the mechanical and dynamical properties of dense biological tissues, describing the tissue as a network of polygons. Recently a class of two-dimensional vertex models was shown to exhibit a disordered rigidity transition controlled by the preferred cellular geometry, which was subsequently echoed by experimental findings. An attractive variant of these models uses a Voronoi tessellation to describe the cells, which reduces the number of degrees of freedom as compared the original vertex model. The Voronoi model was also endowed with a non-equilibrium model of cellular motility, leading to rich, glassy behavior. This glassy behavior was suggested to be inextricably linked to an underlying jamming transition. We test this conjecture, exploring the low-effective-temperature limit of the 2D Voronoi model by studying cell trajectories from detailed dynamical simulations in combination with rigidity measurements of energy-minimized disordered cell configurations. We find that the zero-temperature limit of this model has no unjamming transition. We show that this absence of an unjamming transition is intimately linked to the marginality of the model, i.e. the fact that the constraints imposed on cell areas and perimeters precisely balance the number of degrees of freedom in the model. Our work suggests that constraint counting arguments are useful to understand rigidity in a broad class of models of dense biological tissues.

1 Introduction

How does the large-scale behavior of biological tissues emerge from the collective behavior of the individual cells? Tissues and cellular aggregates display a rich variety of complex, non-equilibrium phenomena, and understanding the impact of microscopic cellular interactions on mechanical tissue properties will help to better understand processes ranging from multicellular development to wound healing to cancer mechanisms.[1–3] For example, recent experiments have revealed that collective rigidity transitions in dense tissues are intimately related to an observed change in cell-scale geometric and material parameters,[4–8] and such transitions have been interpreted through the lens of glass-like and jamming transitions.[4–12] Strikingly, although in particulate systems the athermal jamming transition is distinct from both thermal and non-equilibrium dynamical glass transitions,[13–15] it has been suggested that these may coincide in models for dense biological tissues.[12,16]

A successful class of models to describe tissues on the cellular scale are "vertex" models, which describe tissues as polygonal or polyhedral tilings of space.[11,17–26] The degrees of freedom in these models are cell vertices, allowing for complex, non-convex cell shapes. A very recent variant describes a tissue as a Voronoi tessellation of space,[12] where the degrees of freedom are the cell positions (Voronoi centers). This Voronoi constraint greatly simplifies the process of handling cell dynamics, and recent experiments have shown that Voronoi tessellations can approximate epithelial cell shapes reasonably well.[27,28] Although the 2D Voronoi model has enjoyed rapid adoption by many research groups,[16,28–34] fundamental properties of this model, and even its connections with the original vertex model, are still poorly understood.

Both vertex and Voronoi models describe forces on cells by the gradient of an effective energy written in terms of cell shapes. Here, we use a dimensionless form of a commonly used energy functional:[11,12,20,21,26]

$$e = \sum_{i=1}^{N} \left[k_A \left(a_i - a_0\right)^2 + \left(p_i - p_0\right)^2 \right]. \qquad (1)$$

This energy is a function of the areas a_i and perimeters p_i of the N cells in the system. The parameter k_A controls the cell area stiffness as compared to the perimeter stiffness, and the preferred values for cell area and perimeter are a_0 and p_0, respectively. We define the unit of length such that the average cell area is $\langle a_i \rangle = 1$.

[a] Department of Physics, Syracuse University, Physics Building, Syracuse, New York 13210, USA
‡ DMS and MM contributed equally to this work.
* dmsussma@syr.edu mmerkel@syr.edu

The 2D *vertex* model exhibits a disordered rigidity transition controlled by the preferred perimeter at p_0 at $p_c \equiv 3.81$,[11] which corresponds to the perimeter of a regular unit-area pentagon. This transition, which was successfully compared with experimental data on asthmatic airway epithelia, was identified by studying the athermal energy landscape of the model. In contrast, a recent series of papers has studied rigidity in the 2D *Voronoi* model using non-equilibrium dynamics with cellular self-propulsion.[12,16,30–34] This 2D self-propelled Voronoi (2D-SPV) model exhibits a glass-like dynamical transition in the limit of low motility at $p_0 \approx 3.81$.[12] This surprising result was taken to imply that the athermal 2D Voronoi model also has a rigidity transition at this point,[16] although such a transition was not directly measured. In the context of particulate systems such a coincidence between a dynamical glass and a structural jamming transition would be particularly surprising.[15]

In particulate models the jamming transition can be helpfully interpreted through the lens of "Maxwell" or constraint counting.[35] This approach considers the balance between a model's degrees of freedom and its constraints. For instance, in soft sphere systems a small change in the density can lead to large changes in the number of contacts, where each contact serves as a constraint. The jamming transition occurs when the system is *marginal*, with contacts and degrees of freedom exactly balanced.[35,36] Although much of the work on Maxwell counting has considered simple pairwise interactions, the formulation by Calladine can also be directly applied to systems with many-body quadratic interactions like in vertex and Voronoi models.[37]

In this framework one would expect clear differences between classical jamming models and the various vertex and Voronoi models. In the 2D vertex and 3D Voronoi models the number of degrees of freedom is always larger than the number of constraints represented by Eq. 1 (or its 3D counterpart). These models are *under-constrained*, and are rigidified only by the collective onset of residual stresses, which create additional *effective* constraints.[38] A similar residual-stress-controlled transition has been observed in under-constrained fiber models, and we speculate that such systems may constitute a distinct type of rigidity from the classical jamming transition.[39–41]

In stark contrast, even before considering the effect of residual stress, the 2D Voronoi model is *always marginal*. Note that throughout the manuscript, consistent with past literature we use the terms "under-constrained" and "marginal" without considering any residual-stress-induced effective constraints. Each cell has an area and a perimeter spring in Eq. 1, and so the $2N$ constraints precisely balance the $2N$ degrees of freedom provided by the Voronoi cell centers. As a consequence of this balance, one might expect that the 2D Voronoi model lacks *any* athermal rigidity transition – there is no parameter regime that in particulate jamming would correspond to an under-constrained "floppy" phase.

In this work we directly test whether the 2D Voronoi models shares an athermal unjamming transition with the 2D vertex model. We first study the shear modulus of energy-minimized states and find that it is always positive, showing that all energy minima of the 2D Voronoi model are rigid. We connect this to the marginality of the model by studying the density of vibrational modes. We also perform very-low motility simulations of the 2D-SPV model and show that our results are consistent with a distinction between the dynamical glass transition and the zero-temperature behavior. We close by discussing the $k_A = 0$ limit of the model, which both is under-constrained and has a rigidity transition like the 2D vertex and 3D Voronoi models. This underlines that constraint counting without considering residual stresses provides a useful framework for understanding the differences between various models for dense biological tissues.

2 Models and methods

We begin with 100 initial configurations for each parameter pair (k_A, p_0), which we create by placing N cells at random positions and relaxing the system with periodic boundary conditions and fixed box dimensions. Note that for fixed box dimensions and in the monodisperse case where the preferred area a_0 is the same for all cells, the parameter a_0 does not affect our results. It simply acts as an offset to the overall pressure of the system,[29,32,38] and we set it to $a_0 = \langle a_i \rangle = 1$.

Finding disordered energy minima at large p_0 is highly nontrivial. We used a combination of simple gradient minimization with an adaptive step size, conjugate gradient, Newton-Raphson, and FIRE minimization,[42] but all of these techniques failed to consistently obtain energy-minimized states for $p_0 \gtrsim 3.87$ (notably, for the range $p_0 < 3.84$ which includes the previously reported transition point, more than 98% of minimizations at $k_A = 1$ were successful). This failing is related to the stabilization of many-fold vertices in the ground states of the 2D Voronoi model, which leads to a very cusp-like energy landscape. Stable many-fold vertices were already observed in a thermal version of the Voronoi model,[29,43] despite being unstable in the 2D vertex model.[21,44] Below we restrict our numerical data to the $p_0 < 3.87$ regime, and comment on the high-p_0 regime in the discussion.

For each energy minimized state we analytically compute the bulk modulus b and the shear modulus g based on the dynamical matrix,

$$\mathbf{D}_{ij} = \frac{\partial^2 e}{\partial \boldsymbol{r}_i \partial \boldsymbol{r}_j}, \tag{2}$$

where $\boldsymbol{r}_i$ denotes the vector position of cell i. We analytically compute the matrix elements of $\mathbf{D}$ and diagonalize it to obtain its eigenvalues λ_q with the associated eigenvectors $\boldsymbol{u}_{qi}$. The shear modulus g is computed via[38]

$$g = \frac{1}{N}\left(\frac{\partial^2 e}{\partial \gamma^2} - \sum_q \frac{1}{\lambda_q}\left[\sum_i \frac{\partial^2 e}{\partial \gamma \partial \boldsymbol{r}_i} \cdot \boldsymbol{u}_{qi}\right]^2\right). \tag{3}$$

Here γ is the shear degree of freedom, the outer sum is over all nonzero eigenvalues λ_q, the inner sum is over all cells i, and the dot denotes the scalar product. The bulk modulus b is computed analogously, where the shear degree of freedom γ is replaced by the total area of the system, and the prefactor of $1/N$ is replaced by the dimensionless system area N.

Note that an alternative way to write the dynamical matrix in terms of derivatives of cell areas a_i and perimeters p_i with respect to cell positions allows to more explicitly discuss the influence of

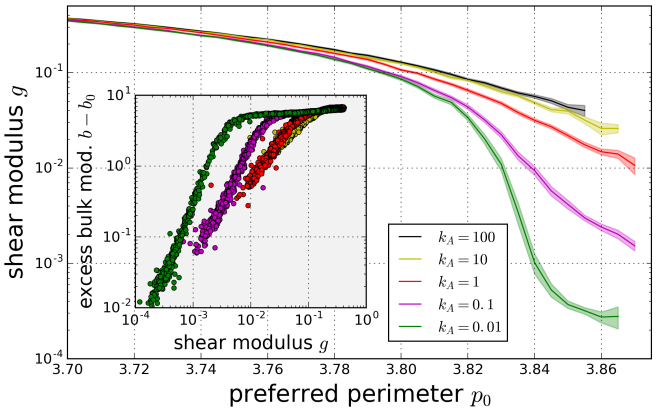

Fig. 1 The shear modulus g is strictly positive over the entire range of model parameters studied. Here it is plotted versus preferred perimeter p_0 for increasing area moduli k_A (bottom to top) in systems of $N = 1024$ Voronoi cells. The shaded regions indicate the standard error of the mean. (inset) Scatter plot of the excess bulk modulus $b - b_0$ with $b_0 = 2k_A$ over the shear modulus g. Each dot corresponds to an energy-minimized configuration.

residual stresses on the elastic properties of the system via the rank of $\mathbf{D}_{ij}$:[38]

$$\mathbf{D}_{ij} = 2\sum_k \left[\frac{\partial p_k}{\partial \boldsymbol{r}_i}\frac{\partial p_k}{\partial \boldsymbol{r}_j} + k_A \frac{\partial a_k}{\partial \boldsymbol{r}_i}\frac{\partial a_k}{\partial \boldsymbol{r}_j} + (p_k - p_0)\frac{\partial^2 p_k}{\partial \boldsymbol{r}_i \partial \boldsymbol{r}_j} + k_A(a_k - a_0)\frac{\partial^2 a_k}{\partial \boldsymbol{r}_i \partial \boldsymbol{r}_j} \right] \tag{4}$$

Classical constraint counting is based on first derivatives of generalized springs – in our case areas and perimeters – which appear in the first two terms in them sum in the above expression. Analogously with work on stressed spring networks,[45] there are also terms proportional to the perimeter and area stress of each cell, which may create additional effective constraints.[38]

To corroborate the qualitative implications of some of our findings in the energy minimized states, we have also performed extensive dynamical simulations. We simulate the 2D-SPV equations of motion,

$$\frac{\mathrm{d}\boldsymbol{r}_i}{\mathrm{d}t} = \boldsymbol{f}_i + v_0 \boldsymbol{n}_i \tag{5}$$

using a simple Eulerian scheme with a time step of $\Delta t = 0.01$. The force on cell i is given by $\boldsymbol{f}_i = -\nabla_i e$ with e from Eq. 1, the parameter v_0 is a self-propulsion speed, and $\boldsymbol{n}_i$ is a polarization vector assigned to every cell i which diffuses on the unit circle with rotational diffusion constant D_r.[12,46]

3 Results

3.1 No athermal transition in the generic 2D Voronoi model

In Fig. 1 we plot the shear modulus g of energy-minimized configurations as a function of p_0, averaged over all successfully minimized states for each parameter pair (k_A, p_0). For every minimized state we observe a strictly positive shear modulus which directly shows that there is no athermal unjamming transition as p_0 is increased. This is in contrast to the conjectured connection between rigidity transitions in the 2D Voronoi and vertex models.[16] Despite the identical energy functional and the similarity of configurations deep in the solid phase,[12,27] the models thus have starkly different low-temperature properties close to the vertex model transition point p_c.

To further quantify the rigidity of these states, we also studied the bulk modulus b in excess of the baseline bulk modulus $b_0 = 2k_A$, the expected value in a fluid regime where all preferred cell perimeters are comfortably met. We find that the excess bulk modulus never vanishes (Fig. 1 inset), so that for the entire parameter regime of the model the bulk modulus is larger than would be expected in such a fluid regime. Surprisingly, we also find that the relationship between the shear and excess bulk modulus is strongly dependent on k_A, with $(b - b_0) \sim g^x$ for exponents $x \approx 1 \ldots 1.5$ at small values of g. This dependence of the exponent on the spring constants is unusual in the context of classical soft-sphere jamming,[47,48] and may be an interesting avenue of future research.

This lack of a mechanically floppy phase is also reflected in the eigenvalue structure of the dynamical matrix $\mathbf{D}$. Most importantly, we find that the only zero-energy modes of the dynamical matrix correspond to the two (trivial) translational modes. Thus, in the athermal 2D Voronoi model there are no available modes for cell rearrangements without energetic cost. This, again, is in contrast with the 2D vertex model, where the energy landscape becomes flat in many directions in the fluid regime (i.e., $p_0 > p_c$), corresponding to a large number of non-trivial zero modes.[11,26]

In Fig. 2a,b we plot the density of states $D(\omega)$ of the dynamical matrix with respect to the frequencies $\omega_q = \sqrt{\lambda_q}$. Consistent with our previous findings on the shear modulus, all changes in $D(\omega)$ are smooth across the entire range of p_0 studied. The peaks in $D(\omega)$ at small p_0 are plane-wave excitations, which we verified by direct visualization, mode counting, and by computing the lowest plane-wave excitation frequencies from the measured shear modulus g (red dashed lines in Fig. 2b). At higher p_0 these modes hybridize with the population of disordered low-frequency modes. Here too the process is smooth, with no indication of a rigidity transition.

To highlight the connection between the 2D Voronoi model and other marginal constraint counting systems, we also examine the "unstressed network" part[49] of $\mathbf{D}$. This ignores the effect of residual stresses on the energy derivatives, and can be computationally accomplished simply by temporarily pretending that the each preferred cell parameter is equal to the current state of that cell. We see in Fig. 2c that there is a plateau of modes extending to seemingly arbitrarily low frequencies. This is reminiscent of particulate models close to the jamming transition,[45] and we interpret this feature as a consequence of the 2D Voronoi model's proximity to a marginal constraint counting point.

3.2 Dynamical simulations in the low-motility regime

How should the lack of an athermal unjamming transition in the 2D Voronoi model be reconciled with the glassy dynamical transition at $p_0 \approx 3.81$ that was previously observed by Bi et al. in the low-motility limit?[12] There the dynamical transition was quanti-

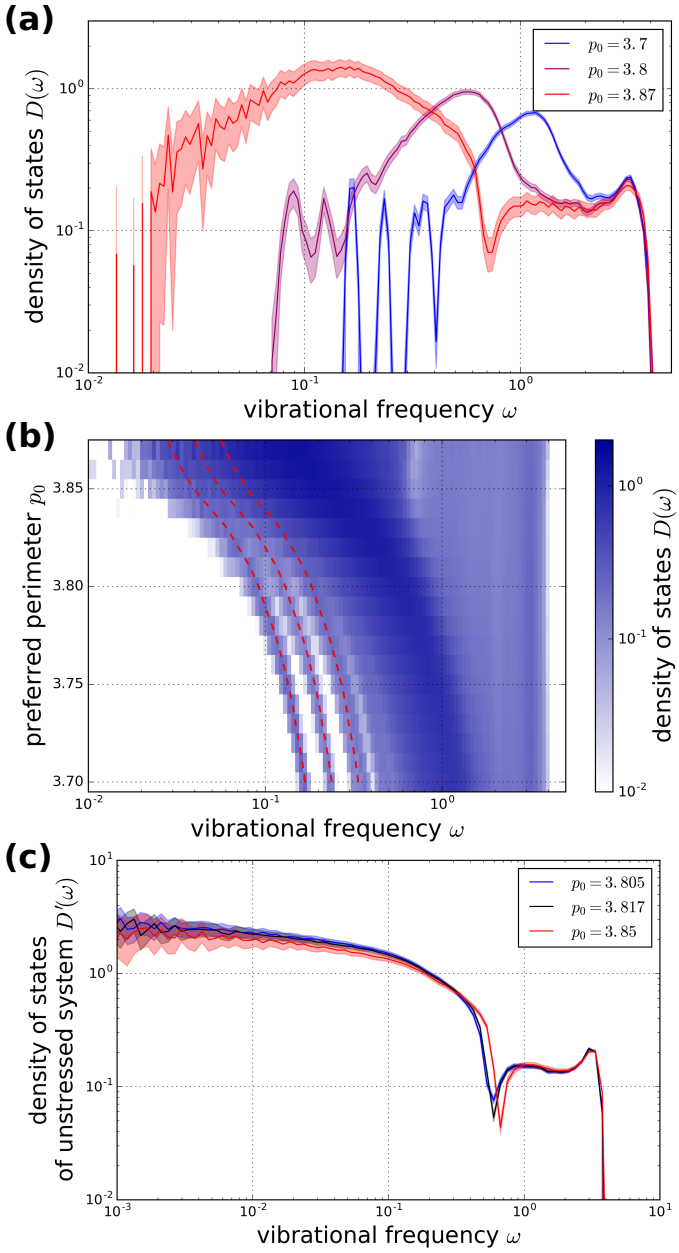

Fig. 2 The density of vibrational modes shows no signs of a sharp transition at finite p_0. (a) Density of states $D(\omega)$ for energy-minimized states with $k_A = 1$ and system size $N = 512$. From left to right the curves correspond to decreasing p_0. (b) Color intensity plot of $D(\omega)$ for $p_0 = 3.7 - 3.87$. The red dashed lines are the lowest-energy plane-wave excitations with frequencies $\omega_n = 2\pi\sqrt{ng/N}$ with $n = 1, 2, 4$, computed using the measured shear modulus g. (c) Density of states $D'(\omega)$ corresponding to the unstressed part of the dynamical matrix for energy-minimized states with $k_A = 1$ and system size $N = 1024$.

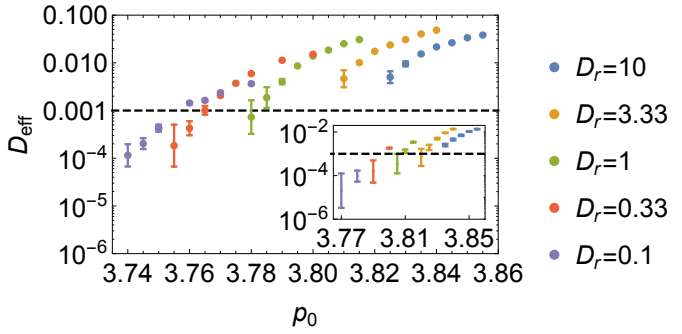

Fig. 3 The dynamical transition point does not converge to a single value at low effective temperatures. The effective diffusion coefficient $D_{\rm eff}$ of the 2D-SPV model for $v_0 = 0.1$ and (inset) $v_0 = 0.05$ is plotted versus p_0, measured at $t = 5 \times 10^5$ for a system size $N = 5000$. The error bars are the standard error of the mean, and the dashed horizontal lines correspond to the cutoff value of $D_{\rm eff} = 10^{-3}$ suggested in previous work.[12]

fied in terms of an effective diffusion constant,

$$D_{\rm eff} \equiv \lim_{t\to\infty} \frac{\langle \Delta r^2(t) \rangle}{(4tD_0)} \tag{6}$$

with $D_0 = v_0^2/(2D_r)$, and it was found that $D_{\rm eff}$ consistently crossed a threshold value close to the same value of $p_0 = 3.81$.[12] However, in light of the above results, such a glass-like transition cannot be due to an underlying jamming transition of the 2D Voronoi model.

To resolve this issue, we use a recently developed GPU-based simulation package[50,51] to repeat the measurements of the effective diffusion constant in the 2D-SPV model, but at a much greater resolution and numerical precision than was previously accessible (with orders of magnitude improvement in both the total simulation length and system size). In contrast with previous results, we find that $p_0 = 3.81$ no longer plays a special role, and further that the implied dynamical transition is a strong function of D_r (Fig. 3). Hence, simulating for much longer times suggests the absence of a unique low-temperature transition point for the 2D-SPV model, thus corroborating the absence of an unjamming transition in the athermal 2D Voronoi model.

3.3 Existence of a rigidity transition in the $k_A = 0$ limit

To further test whether the absence of a rigidity transition is related to the marginality of the 2D Voronoi model, we now alter the constraint counting by setting the area elasticity to zero: $k_A = 0$. This removes the area constraints in Eq. 1 and creates an *under-constrained* model with $2N$ degrees of freedom but only N constraints. Indeed, we find that in this limit the 2D Voronoi model *does* possess an athermal unjamming transition, with a continuous transition in the shear modulus g and a discontinuous transition in the bulk modulus b (Fig. 4a; note that $b_0 = 0$ in this case). Looking back at the general $k_A > 0$ case (Fig. 1), we see that for very low k_A both the shear and excess bulk modulus drop by approximately two orders of magnitude at values of p_0 close to the $k_A = 0$ transition, but remain finite as expected from the constraint counting. Taken together, this confirms that a jamming-based constraint counting perspective helps predict the

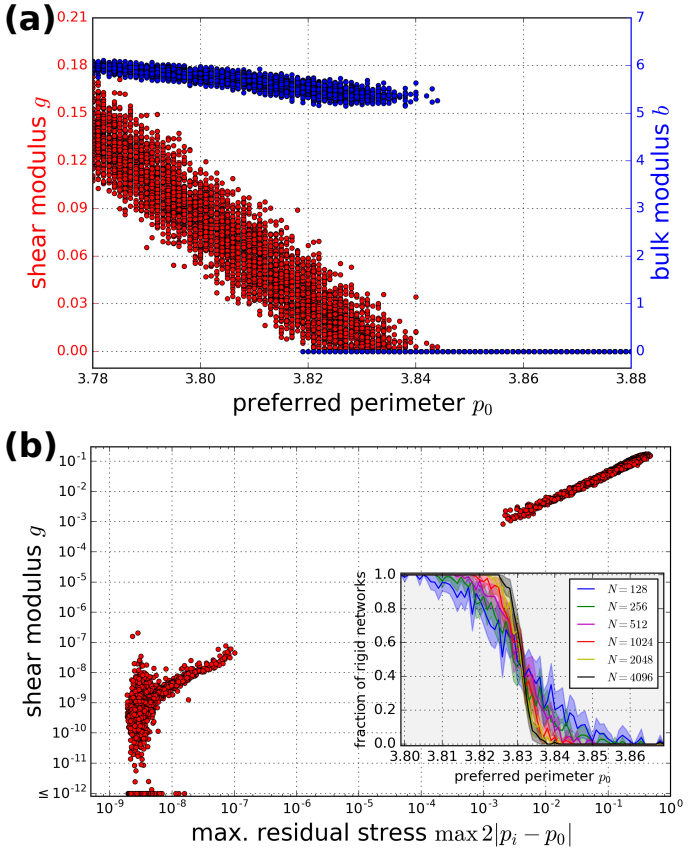

Fig. 4 The under-constrained $k_A = 0$ limit of the 2D Voronoi model shows a residual-stress-controlled rigidity transition. (a) The transition is continuous in the shear modulus g and discontinuous in the bulk modulus b. Each dot represents one energy-minimized configuration. (b) The shear modulus g is plotted versus the maximal magnitude of residual stresses, given by twice the maximal deviation of cell perimeters p_i from p_0. A clear separation between solid configurations with finite residual stresses and floppy configurations without residual stresses is visible (the inset does not cover any data points). (inset) Quantification of the $k_A = 0$ transition point based on the fraction of rigid, energy-minimized states as a function of p_0 for varying system size N.

mechanical properties of both vertex and Voronoi models.

This puts the special $k_A = 0$ limit in a similar class as the 3D Voronoi and 2D vertex models, both of which are under-constrained and possess an athermal unjamming transition. In particular, in the 3D Voronoi model residual stresses are both necessary and sufficient to rigidify the system.[38] We find that this is also true in the $k_A = 0$ limit of the 2D Voronoi model: the occurrence of residual stresses is perfectly correlated with rigidity (Fig. 4b).

To precisely determine the value of the transition in the limiting case $k_A = 0$, we plot the fraction of rigid networks in the inset to Fig. 4b. For these states minimized with a simple gradient descent algorithm, we found that the average transition point $p_0^* = 3.831 \pm 0.001$ did not depend significantly on system size. However, when minimizing with the FIRE algorithm we obtained a significantly different transition point of $p_0^* \approx 3.80$ (data not shown). Note that such a sensitivity of the transition point to the minimization protocol is consistent with a landscape that possesses a large number of very small energy barriers, emphasizing the need for high-precision numerical studies.

4 Summary

Our work emphasizes the role of the precise nature of a model's degrees of freedom in determining its properties, even among models using *identical* cell-shape-based energy functionals.[11,12,33,38,43,52] Here we have found that the 2D Voronoi model governed by Eq. 1 does not have a zero-temperature rigidity transition, with solid behavior found throughout the entire range of p_0 studied. Although we were not able to obtain energy-minimized states for target perimeters $p_0 \gtrsim 3.87$, the p_0 range studied easily covers the dynamic transition point at $p_0 \approx 3.81$ previously observed in the 2D-SPV and vertex models.[11,12,26]

Moreover, the existence of a mechanically floppy regime for $p_0 \gtrsim 3.87$ is theoretically disfavored. As noted above, the 2D Voronoi model is marginal: its $2N$ degrees of freedom are precisely balanced by $2N$ constraints imposed by the area and perimeter springs in Eq. 1. Consistent with earlier work,[29] we additionally observe the stabilization of four-fold vertices in the high-p_0 regime, and each of these effectively adds a constraint, shifting the system *further towards rigidity*. The only way this could lead to a loss of rigidity is if a number of constraints became redundant,[36] an improbable result given the disordered geometry of the problem. Hence, we view the existence of a fluid regime at high p_0 in the athermal limit as very unlikely.

Note that previous work[12] already contains hints that states in the reported fluid regime of the 2D-SPV model may be solid in the athermal limit. For instance, for simulations performed at $p_0 = 3.85$ the mean-squared displacement had a notable regime of sub-diffusive behavior,[12] suggesting caging with finite energy barriers to rearrangement.

This conclusion is further supported by our dynamical simulations of the 2D Voronoi model. With significantly increased simulation time and system size as compared to previous work,[12] our simulation results strongly suggest a scenario in which a dynamic glass transition is a function of the rotational diffusion; this is in contrast to previously reported results,[12] but it is consistent with the decoupling of the glass and jamming transitions observed in self-propelled particle models.[15] Taken together, this suggests that the glass-like transition reported for the 2D-SPV model does not coincide with an underlying athermal jamming transition, and highlights the need to understand the glass-like properties of the Voronoi model in more detail.[53]

A consistent picture of the low-temperature properties of a broad range of cell-based models emerges based on the unstressed constraint counting of the model. In under-constrained models, such as the 2D vertex and 3D Voronoi model, both a rigid and a floppy phase exist as a consequence of the residual stresses that the models can support.[11,38,54] Here we show that in the 2D Voronoi model with $k_A > 0$, which is marginal in the absence of residual stresses, there is no mechanically floppy phase. In contrast, the special case of $k_A = 0$, which is under-constrained in the absence of residual stresses, shows both a floppy and a rigid regime, where rigidity is induced by residual stresses just as in the 2D vertex and 3D Voronoi models. Thus, although residual

stress can contribute additional effective constraints, even constraint counting without considering these effective constraints allows one to make predictions about the presence and nature of rigidity transitions in these tissue models.

This connection suggests that the rigidity transitions observed in the 2D vertex and 3D Voronoi model can be destroyed by adding more constraints. From this point of view, the 2D Voronoi model could be considered as a type of vertex model where additional constraints have been introduced to force every cell to assume the shape of a local Voronoi volume.[32] These additional constraints are one way to bring the model to marginality, but one could imagine adding other types of constraints that affect the constraint counting of the vertex model.[53]

The works suggests natural avenues for future study, particularly with respect to the unusual underlying energy landscape of dense tissue models. We found rigid ground state configurations for all target perimeters in the $k_A > 0$ Voronoi model, but we have not probed the energy barriers associated with either single-cell displacements or collective, low-frequency excitations. Studying these energy barriers is a natural probe of the nonlinear mechanical response of these systems, and the precise nature of the distribution of low energy barriers in the very weak solid that we find in the high-p_0 regime will be of great importance in understanding the low-effective-temperature limit of the 2D-SPV model.

The fact that the transition point in the $k_A = 0$ limit depends sensitively on the minimization method indicates that the sampling of disordered states is important. In this paper, we quenched to zero temperature from states with cell positions drawn from a uniform random distribution, i.e. infinite temperature configurations. Preliminary results on finite-temperature quenches showed smaller, yet still non-zero shear moduli for $k_A > 0$. Thus, while the conclusions of our work remain unaltered, it may be interesting to systematically study this dependence of rigidity on configurational sampling and its connection with the underlying energy landscape.

Finally, although we do not find a sharp transition in the 2D Voronoi model, it is still intriguing that both the elastic moduli at zero temperature and the finite-activity diffusion constants change by orders of magnitude in the regime close to $p_0 = 3.8 \pm 0.1$, which is suggestive of a deeper link to the transition observed in the vertex model at $p_c = 3.81$. The fact that both the $k_A = 0$ limit of the Voronoi model and the vertex model *do* possess a transition at nearby values of p_0 suggests that the behavior of the Voronoi model for $k_A > 0$ may be controlled by its proximity to these avoided transitions. This suggests that, in analogy with the 3D Voronoi transition,[38] a disordered geometric minimal perimeter may be relevant in thinking about all of the 2D models. The existence of such a minimal perimeter could also provide a robust mechanism that explains the value of $p_c = 3.81$ seen in experiments.[6,31]

We thank Lisa Manning and Cristina Marchetti for fruitful discussions and comments on this manuscript. This work was supported by NSF-POLS-1607416 (DMS), the Alfred P. Sloan Foundation, the Gordon and Betty Moore Foundation, and the Research Corporation for Scientific Advancement (MM); we acknowledge computing support through NSF ACI-1541396, and the Tesla K40 used for this research was donated by the NVIDIA Corporation.

References

1 P. Friedl and D. Gilmour, *Nature reviews. Molecular cell biology*, 2009, **10**, 445–457.
2 A. Brugués, E. Anon, V. Conte, J. H. Veldhuis, M. Gupta, J. Colombelli, J. J. Muñoz, G. W. Brodland, B. Ladoux and X. Trepat, *Nature Physics*, 2014, **10**, 683–690.
3 R. Etournay, M. Popović, M. Merkel, A. Nandi, C. Blasse, B. Aigouy, H. Brandl, G. Myers, G. Salbreux, F. Jülicher and S. Eaton, *eLife*, 2015, **4**, e07090.
4 T. E. Angelini, E. Hannezo, X. Trepat, M. Marquez, J. J. Fredberg and D. a. Weitz, *Proceedings of the National Academy of Sciences*, 2011, **108**, 4714–4719.
5 M. Sadati, N. Taheri Qazvini, R. Krishnan, C. Y. Park and J. J. Fredberg, *Differentiation*, 2013, **86**, 121–125.
6 J.-A. Park, J. H. Kim, D. Bi, J. A. Mitchel, N. T. Qazvini, K. Tantisira, C. Y. Park, M. McGill, S.-H. Kim, B. Gweon *et al.*, *Nature materials*, 2015, **14**, 1040–1048.
7 S. Garcia, E. Hannezo, J. Elgeti, J.-F. Joanny, P. Silberzan and N. S. Gov, *Proceedings of the National Academy of Sciences*, 2015, **112**, 15314–15319.
8 C. Malinverno, S. Corallino, F. Giavazzi, M. Bergert, Q. Li, M. Leoni, A. Disanza, E. Frittoli, A. Oldani, E. Martini, T. Lendenmann, G. Deflorian, G. V. Beznoussenko, D. Poulikakos, K. H. Ong, M. Uroz, X. Trepat, D. Parazzoli, P. Maiuri, W. Yu, A. Ferrari, R. Cerbino and G. Scita, *Nature Materials*, 2017, **16**, 587–596.
9 E.-M. Schotz, M. Lanio, J. a. Talbot and M. L. Manning, *Journal of The Royal Society Interface*, 2013, **10**, 20130726–20130726.
10 J. J. Fredberg, *Physiology*, 2014, **29**, 218–219.
11 D. Bi, J. Lopez, J. Schwarz and M. L. Manning, *Nature Physics*, 2015, **11**, 1074–1079.
12 D. Bi, X. Yang, M. C. Marchetti and M. L. Manning, *Phys. Rev. X*, 2016, **6**, 021011.
13 A. Ikeda, L. Berthier and P. Sollich, *Physical review letters*, 2012, **109**, 018301.
14 Y. Fily, S. Henkes and M. C. Marchetti, *Soft matter*, 2014, **10**, 2132–2140.
15 L. Berthier, *Physical review letters*, 2014, **112**, 220602.
16 X. Li, A. Das and D. Bi, *arXiv preprint arXiv:1608.06334*, 2016.
17 H. Honda, *J. Theor. Biol.*, 1978, **72**, 523–530.
18 T. Nagai and H. Honda, *Philosophical Magazine Part B*, 2001, **81**, 699–719.
19 L. Hufnagel, A. A. Teleman, H. Rouault, S. M. Cohen and B. I. Shraiman, *Proc. Natl. Acad. Sci. USA*, 2007, **104**, 3835–3840.
20 R. Farhadifar, J.-C. Röper, B. Aigouy, S. Eaton and F. Jülicher, *Curr. Biol.*, 2007, **17**, 2095–2104.
21 D. B. Staple, R. Farhadifar, J. C. Röper, B. Aigouy, S. Eaton and F. Jülicher, *Euro. Phys. J. E*, 2010, **33**, 117–127.
22 G. R. Miriams et al., *PLoS Comput. Biol.*, 2013, **9**, e1002970.
23 A. G. Fletcher, M. Osterfield, R. E. Baker and S. Y. Shvartsman, *Biophys. J.*, 2014, **106**, 2291–2304.
24 S. Alt, P. Ganguly and G. Salbreux, *Phil. Trans. R. Soc. B*, 2017, **372**, 20150520.
25 A. Hočevar and P. Ziherl, *Phys. Rev. E*, 2009, **80**, 011904.
26 D. Bi, J. H. Lopez, J. M. Schwarz and M. L. Manning, *Soft Matter*, 2014, **10**, 1885–1890.
27 S. Kaliman, C. Jayachandran, F. Rehfeldt and A.-S. Smith, *Frontiers in Physiology*, 2016, **7**,.
28 T. Vazquez-Faci, R. van Drongelen, M. van der Zee and T. Idema, *arXiv:1705.06205*, 2017.
29 T. Su and G. Lan, *arXiv preprint arXiv:1610.04254*, 2016.
30 F. Giavazzi, M. Paoluzzi, M. Macchi, D. Bi, G. Scita, M. L. Manning, R. Cerbino and M. C. Marchetti, *arXiv preprint arXiv:1706.01113*, 2017.
31 L. Atia, D. Bi, Y. Sharma, J. A. Mitchel, B. Gweon, S. A. Koehler, S. J. DeCamp, B. Lan, J. H. Kim, R. Hirsch *et al.*, *Nature Physics*, 2018, 1.
32 X. Yang, D. Bi, M. Czajkowski, M. Merkel, M. L. Manning and M. C. Marchetti, *Proceedings of the National Academy of Sciences*, 2017, **114**, 12663–12668.

33 D. L. Barton, S. Henkes, C. J. Weijer and R. Sknepnek, *PLoS Computational Biology*, 2017, **13**, e1005569.

34 Y.-W. Li and M. P. Ciamarra, *arXiv*, 2017.

35 A. J. Liu and S. R. Nagel, *Annual Review of Condensed Matter Physics*, 2010, **1**, 347–369.

36 T. Lubensky, C. Kane, X. Mao, A. Souslov and K. Sun, *Reports on Progress in Physics*, 2015, **78**, 073901.

37 C. Calladine, *International Journal of Solids and Structures*, 1978, **14**, 161–172.

38 M. Merkel and M. L. Manning, *New Journal of Physics*, 2018, **20**, 022002.

39 A. Sharma, A. Licup, K. Jansen, R. Rens, M. Sheinman, G. Koenderink and F. MacKintosh, *Nature Physics*, 2016, **12**, 584.

40 M. F. Vermeulen, A. Bose, C. Storm and W. G. Ellenbroek, *Physical Review E*, 2017, **96**, 053003.

41 N. Noll, M. Mani, I. Heemskerk, S. J. Streichan and B. I. Shraiman, *Nature Physics*, 2017, **13**, 1221.

42 E. Bitzek, P. Koskinen, F. Gähler, M. Moseler and P. Gumbsch, *Physical review letters*, 2006, **97**, 170201.

43 D. M. Sussman, J. Schwarz, M. C. Marchetti and M. L. Manning, *Physical Review Letters*, 2018, **120**, 058001.

44 M. A. Spencer, Z. Jabeen and D. K. Lubensky, *Eur. Phys. J. E*, 2017, **40**, 2.

45 M. Wyart, L. E. Silbert, S. R. Nagel and T. A. Witten, *Phys. Rev. E*, 2005, **72**, 051306.

46 S. Henkes, Y. Fily and M. C. Marchetti, *Phys. Rev. E*, 2011, **84**, 040301.

47 C. P. Goodrich, S. Dagois-Bohy, B. P. Tighe, M. van Hecke, A. J. Liu and S. R. Nagel, *Physical Review E*, 2014, **90**, 022138.

48 C. P. Goodrich, A. J. Liu and J. P. Sethna, *Proceedings of the National Academy of Sciences*, 2016, **113**, 9745–9750.

49 S. Alexander, *Physics Reports*, 1998, **296**, 65.

50 D. M. Sussman, *Comput. Phys. Commun.*, 2017, **219**, 400.

51 https://gitlab.com/dmsussman/cellGPU, 2017.

52 M. Chiang and D. Marenduzzo, *EPL (Europhysics Letters)*, 2016, **116**, 28009.

53 D. M. Sussman, M. Paoluzzi, M. C. Marchetti and M. L. Manning, *EPL (Europhysics Letters)*, 2018, **121**, 36001.

54 M. Moshe, M. J. Bowick and M. C. Marchetti, *arXiv preprint arXiv:1708.07848*, 2017.